View metadata, citation and similar papers at core.ac.uk

brought to you by CORE

provided by Syracuse University Research Facility and Collaborative Environment

Syracuse University

SURFACE

Physics College of Arts and Sciences

2003

Low-Mobility Solar Cells: a Device Physics Primer with Application to Amorphous Silicon

Eric A. Schiff

Syracuse University

Follow this and additional works at: https://surface.syr.edu/phy

Part of the Physics Commons

Recommended Citation

"Low-mobility Solar Cells: A Device Physics Primer with Application to Amorphous Silicon," E. A. Schiff, Solar Energy Materials and Solar Cells 78, 567-595 (2003).

This Article is brought to you for free and open access by the College of Arts and Sciences at SURFACE. It has been accepted for inclusion in Physics by an authorized administrator of SURFACE. For more information, please contact surface@syr.edu.

ELSEVIER

Available online at www.sciencedirect.com
SCIENCE DIRECT®

Solar Energy Materials & Solar Cells 78 (2003) 567–595

Solar Energy Materials & Solar Cells

www.elsevier.com/locate/solmat

Low-mobility solar cells: a device physics primer with application to amorphous silicon

E.A. Schiff*

Department of Physics, Syracuse University, Syracuse, New York 13244-1130, USA

Abstract

The properties of *pin* solar cells based on photogeneration of charge carriers into low-mobility materials were calculated for two models. Ideal *p*- and *n*-type electrode layers were assumed in both cases. The first, elementary case involves only band mobilities and direct electron–hole recombination. An analytical approximation indicates that the power in thick cells rises as the $\frac{1}{4}$ power of the lower band mobility, which reflects the buildup of space-charge under illumination. The approximation agrees well with computer simulation. The second model includes exponential bandtail trapping, which is commonly invoked to account for very low hole drift mobilities in amorphous silicon and other amorphous semiconductors. The two models have similar qualitative behavior. Predictions for the solar conversion efficiency of amorphous silicon-based cells that are limited by valence bandtail trapping are presented. The predictions account adequately for the efficiencies of present a-Si : H cells in their "as-prepared" state (without light-soaking), and indicate the improvement that may be expected if hole drift mobilities (and valence bandtail widths) can be improved.
© 2002 Elsevier Science B.V. All rights reserved.

Keywords: Amorphous silicon; Low-mobility solar cells

1. Introduction

In this paper we discuss the device physics of solar cells based on low-mobility materials. Solar cells based on hydrogenated amorphous silicon (a-Si : H) [1–3], on polymers or organic materials [4], and dye-sensitized porous metal-oxide "membranes" [5,6] are examples of such cells. For specificity, we shall define

*Fax: +1-315-443-9103.
E-mail address: easchiff@syr.edu (E.A. Schiff).

0927-0248/03/$ - see front matter © 2002 Elsevier Science B.V. All rights reserved.
doi:10.1016/S0927-0248(02)00452-X

"low-mobility" materials as those in which at least one of the two carrier particles (usually electron and hole) has a characteristic mobility less than $1\,cm^2/V\,s$.

A mobility μ is the ratio $v(F)/F$ of the net drift speed $v(F)$ of a carrier in an electric field F to the field itself. The reason that a low mobility can strongly affect the workings of a solar cell is that the density of slowly drifting carriers builds up substantially under solar illumination. This buildup of carriers (and thus of electrical charge) can dominate the workings of the cell, determining both the maximum useful thickness of the cell as well as the power generated.

In this paper we shall analyze the device physics of low-mobility solar cells for two simple models, and then apply this analysis to estimating the maximum achievable efficiency of solar cells based on hydrogenated amorphous silicon. In the first section we present a discussion of perhaps the simplest conceivable, "trap-free" model of a low-mobility absorber with ideal electrodes. We have included introductory material in this section in an effort to make it reasonably self-contained. We use this model to develop a perspective on low-mobility cells which is applicable for more sophisticated models. Although we shall use computer simulations to illustrate solar cell function throughout this paper, for this simplest model we have found a simple, analytical approximation for the maximum power density P (in Watts/Area) in the limit of a low hole mobility μ_h:

$$P = ((2/3)V_{OC})^{3/2}(\mu_h \varepsilon\varepsilon_0 (eG)^3)^{1/4}. \tag{1}$$

Here V_{OC} is the solar cell's "open-circuit voltage". G is the rate at which carriers are generated by light in the intrinsic layer; G is assumed to be constant throughout this layer. e is the charge of an electron. $\varepsilon\varepsilon_0$ is the dielectric constant of the intrinsic layer material (in SI units).

In a second section we treat an important, particular model for low-mobilities, which is trapping of charge carriers in exponential bandtails. The exponential bandtail model describes mobilities fairly well in several inorganic, non-crystalline semiconductors, and thus provides a better foundation for quantitative work than the simpler, "trap-free" model. For simplicity, we assume that only one carrier, the hole, undergoes bandtail trapping; this assumption applies fairly well to a-Si:H at or above room temperature. We again study the behavior for homogeneous photogeneration of carriers throughout the cell, and we again assume ideal electrodes. The qualitative behavior is fairly similar to that for the "trap-free" case just described.

In the last section we re-analyze the exponential bandtail model under solar illumination, which results in highly non-uniform photogeneration. We use the optical absorption properties of amorphous silicon. We predict the power output of such cells as a function of the valence bandtail width; these predictions are summarized in Fig. 12. We believe that these predictions are a fairly accurate guide to the best power densities that may be achieved in simply engineered solar cells based on a-Si:H, presuming that the difficult problems of achieving ideal electrode layers and suppressing defect formation have been solved.

2. The pin structure without traps

2.1. Preliminaries

The fundamental structure of the solar cells that we consider consists of three layers: a *p*-type electrode layer that collects holes, an intrinsic layer in which photocarriers are generated, and an *n*-type electrode layer to collect electrons. The intrinsic layer is assumed to be an insulator under dark conditions, with negligible dark conductivity. As illustrated in Fig. 1, in this structure excess electrons are actually donated from the *n*-type layer to the *p*-type layer, leaving these layers positively and negatively charged (respectively), and creating a sizable "built-in" electric field.

Light enters the cell as a stream of photons. The photons are mostly absorbed in the intrinsic layer, where (ideally) each photon that is absorbed will generate one electron and one hole photocarrier. The photocarriers are swept away by the built-in electric field to the *n*-type and *p*-type layers, respectively—thus generating solar electricity!

In this section we describe the most basic photoelectric processes in a low-mobility intrinsic layer, along with the associated parameters that are used in modeling semiconductor devices. We shall not present any equivalent discussion for the electrode layers, which we shall assume are "ideal" and have no effect on the behavior of the cell. Of course, achieving such ideal electrodes may be difficult in practice. Fig. 2 is a graph that is often used to illustrate the photoelectric processes in an intrinsic layer. The vertical axis indicates the energy for electronic levels; the horizontal axis represents one dimension (x) of ordinary space. The horizontal lines labeled E_C and E_V indicate the energies of the conduction and valence bandedges. In this model, electrons can only occupy conduction band states that have level energies larger than E_C; these states are indicated by the shaded area above E_C. The average speed v_e of these electrons in an electric field F is characterized by the electron mobility μ_e (cm^2/V s):

$$v_e = \mu_e F. \tag{2}$$

Similarly, holes can only occupy states below E_V, and their average speed is given by their mobility μ_h.

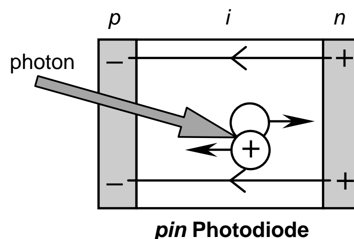

Fig. 1. The *pin* diode structure.

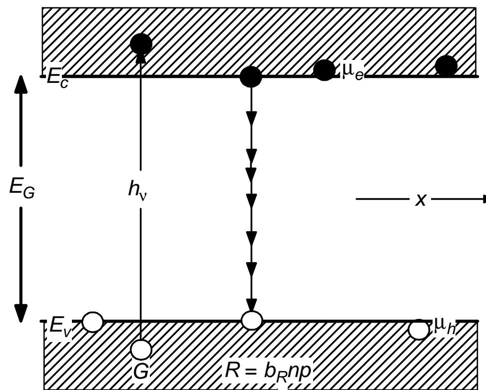

Fig. 2. Cartoon illustrating the principal parameters used in modeling photocarriers in semiconductors: bandedge level energies E_C and E_V, bandgap E_G, interband photocarrier generation G, electron and hole mobilities μ_e and μ_h and densities n and p, and electron–hole recombination R.

In a *pin* solar cell, electrons and holes are mostly generated by photons with energies $h\nu$ (eV) that are greater than the *bandgap* $E_G = E_C - E_V$. A photon excites an electron out of the filled electronic levels in the valence band and into the conduction band; the photoexcited electron leaves one hole behind in the valence band.

The *generation rate* at which electrons (and holes) are generated by the incident flux of photons will be denoted G ($\mathrm{cm^{-3}\,s^{-1}}$). Once these electrons and holes are generated, they first "thermalize". Initially, an electron will occupy an energy level somewhat above the conduction bandedge; similarly, the hole will occupy a level somewhat below the valence bandedge. They each rapidly shed energy and coalesce onto the levels rather close (roughly within the thermal energy kT) to the bandedges.

In the present model, once this thermalization has occurred, the electrons and holes can only *recombine* with each other. We shall consider a slightly more elaborate model including "trapping" effects later on. The corresponding recombination rate R of electrons with holes is usually assumed to be proportional to the density of electrons n, the density of holes p, and the recombination coefficient b_R ($\mathrm{cm^3\,s^{-1}}$):

$$R = b_R np. \tag{3}$$

Recombination creates a good deal of energy that is either released as heat (i.e. as a shower of phonons) or as a photon.[1] The latter, "radiative" recombination process is uncommon in solar cells—but is intentionally maximized in light-emitting devices.

There are two more essential parameters: these are the "effective densities of states" N_C ($\mathrm{cm^{-3}}$) and N_V ($\mathrm{cm^{-3}}$) of the conduction bandedge and the valence

[1] We are neglecting "Auger" recombination, which is often considered in crystalline semiconductors. In Auger recombination, the energy that is released by recombination of an electron and a hole is taken up by a second electron (or hole); recombination is proportional to n^2p or np^2. I am unaware of any well-documented experiment showing Auger recombination in low-mobility semiconductors, although the possibility should certainly not be excluded.

bandedge, respectively. The importance of these parameters will only emerge in our discussion of the "open-circuit" voltage.

2.2. Current–voltage relations for varying cell thickness

In Fig. 3 we present the calculated current density $J(V)$ as a function of bias voltage for *pin* diode structures under illumination; results are given for several thicknesses of the intrinsic layer. The computer calculations throughout this paper were done using the ©AMPS-PC computer program from Pennsylvania State University [7]. Intrinsic layer parameters are indicated in the caption. We have chosen the hole mobility μ_h to be much less than the electron mobility μ_e both for this figure and for essentially all of the modeling in this paper. The *p*- and *n*-layer parameters were chosen so that these layers are essentially ideal (in the sense that they do not significantly affect the current–voltage relation). We discuss some technicalities of using AMPS PC in Appendix A.

In case the reader is unfamiliar with such J–V graphs, we briefly describe their main attributes. A positive voltage V corresponds to an external electric potential that is larger at the *p*-layer electrode than at the *n*-layer electrode. The value of V for which $J = 0$ is the "open-circuit" voltage V_{OC}, and is the output of the solar cell when it is unloaded by any external circuit. As the voltage is reduced below V_{OC}, the current density is negative, which means that the electrical current flows "uphill" into the positive terminal of the external potential; the energy, which makes this possible, comes from the light absorbed in the cell. At short-circuit (i.e. at $V = 0$ V), the magnitude of the current density is denoted the "short-circuit current density" J_{SC}; of course the actual current measured in a circuit is the product of the current density and the area of the cell.

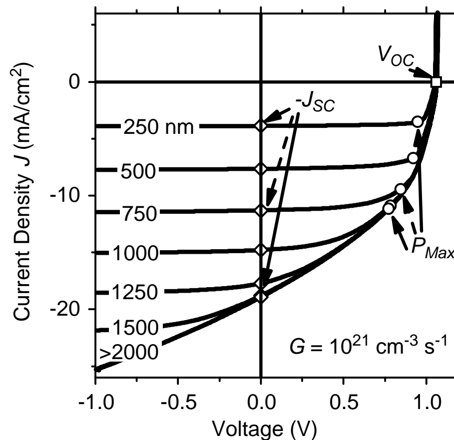

Fig. 3. Computer calculations of the current density J as a function of applied voltage for illuminated *pin* diodes (300 K) with varying *i*-layer thickness. The illumination creates uniform photogeneration G throughout the *i*-layer. Intrinsic layer modeling parameters were $\mu_h = 10^{-2}\,\mathrm{cm^2/V\,s}$, $\mu_e = 20\,\mathrm{cm^2/V\,s}$, $b_R = 10^{-9}\,\mathrm{cm^3/s}$, $E_G = 1.78$ eV, $N_C = N_V = 5 \times 10^{20}/\mathrm{cm^3}$.

No power is delivered to the external circuit under short-circuit or open-circuit conditions. As the voltage across the cell rises from 0 to V_{OC}, a power density $P(V) = -J(V)V$ is delivered to the external circuit. The voltage/current pairs corresponding to the maximum power P_m are indicated in the figure; the maximum power point must be found individually for each cell.

Fig. 4 illustrates how these principal solar cell parameters depend upon the thickness of the intrinsic layer. There are four main features to this figure.

- For the thinner structures ($d < 1250$ nm), the short-circuit current density J_{SC} is essentially proportional to thickness. This aspect is simply a property of the optical absorption model we are using, which assumes a constant generation rate G throughout an absorber layer of arbitrary thickness.

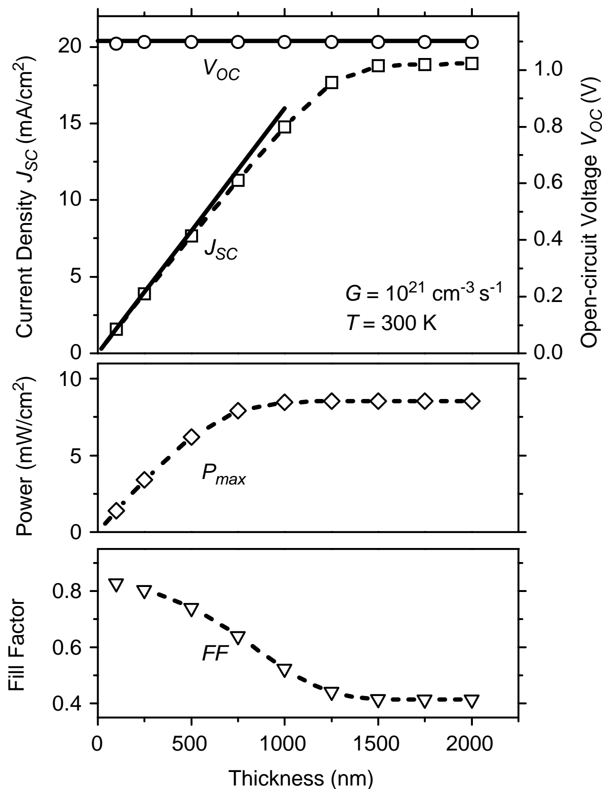

Fig. 4. Computer simulation of the dependence of the main solar cell parameters (open-circuit voltage, short-circuit current density, power density, and fill factor) upon the thickness of the intrinsic layer ($T = 300$ K). The model parameters are the same as for Fig. 3. The solid lines indicate analytical calculations. Note that the open-circuit voltage V_{OC} is nearly thickness-independent. The short-circuit current density J_{SC} is proportional to thickness for thicknesses less than about 1250 nm, and then saturates. The maximum power density from the cell is reached for a smaller thickness around 700 nm, after which it too saturates.

- The open-circuit voltage V_{OC} largely determines the voltage of the solar cell when it is generating power. V_{OC} is nearly independent of thickness, which makes it a particularly fundamental aspect of a solar cell. We shall derive the following formula for V_{OC} in terms of the fundamental parameters of the intrinsic layer material:

$$eV_{OC}^{0} = E_G + kT \ln\left(\frac{G}{b_R N_C N_V}\right). \tag{4}$$

Note that this estimate of V_{OC} is not only independent of thickness, it is independent of the carrier mobilities.

- For intrinsic layers exceeding some collection width d_C, the output power density P of the cell saturates at some maximum value. This is not an optical effect; the actual power absorbed from the optical beam is strictly proportional to the thickness for our model of uniform G. d_C is actually determined by the buildup of an electrical "space-charge" of drifting carriers. In the limit of low hole mobility, we shall obtain the following approximations for the width d_c and the power density generated by the cell:

$$d_C = ((2/3)V_{OC})^{1/2}(\mu_h \varepsilon\varepsilon_0/eG)^{1/4}, \tag{5}$$

$$P = ((2/3)V_{OC})^{3/2}(\mu_h \varepsilon\varepsilon_0 (eG)^3)^{1/4}. \tag{1}$$

Note that these formulae nicely complement the open-circuit voltage formulae, which do not depend on the hole mobility.

- The fill-factor FF, which is defined implicitly from the power relation $P=(\mathrm{FF})J_{SC}V_{OC}$, is a helpful characterization for thinner cells, where it indicates the deviations from the ideal behavior described by $\mathrm{FF}=0.91$. It is less useful for thicker cells. As can be seen in Fig. 4, the fill-factor saturates at about the same thickness as the short-circuit current density, having fallen to a value around 0.4. The power density saturates for cells that are thinner than is required for J_{SC} and the fill factor to saturate; we discuss the reasons in Section 2.8.

2.3. Analytical estimate for current density in thin cells

For very thin cells under short-circuit conditions, we can safely assume that every photocarrier that is generated by photon absorption will be swept across the absorber layer by the internal electric field and collected. Electrons will be swept into the *n*-layer, and holes into the *p*-layer, respectively. During this collection process, electric charge moves through the external circuit that sets the voltage across the cell; this external current balances the charge motion within the cell. The equation describing the current is then:

$$J_{SC} = eGd, \tag{6}$$

where $e = 1.6 \times 10^{-19}$ C is the electronic charge. The values predicted using this equation and $G = 10^{21}$ cm^{-3} are shown as the solid line in Fig. 4. They provide a very satisfactory explanation for the short-circuit current density that was calculated using the full simulation for thinner cells, and indeed one may think of the agreement as a test of the simulation program.

2.4. V_{OC} and quasi-Fermi levels: a theorem

An analytical approximation to the open-circuit voltage V_{OC} may be obtained using a remarkable, if difficult to prove, theorem. The theorem is expressed in terms of quasi-Fermi levels, which are defined as follows. If the mobile electron density (the density of electrons occupying levels above the conduction bandedge E_C) is denoted n, then the electron quasi-Fermi level E_{Fn} is defined:

$$E_{Fn} \equiv E_C + kT \ln\left(\frac{n}{N_C}\right), \tag{7}$$

where N_C is the conduction bandedge density-of-states. As similar expression defines the hole quasi-Fermi level E_{Fp} in terms of the mobile hole density p,

$$E_{Fp} \equiv E_V - kT \ln\left(\frac{p}{N_V}\right). \tag{8}$$

Quasi-Fermi levels are often introduced in semiconductor device modeling [8,9]. They have the property that electron and hole currents may be conveniently expressed in terms of gradients; thus the electrical current density from electrons J_n may be written

$$J_n = -n\mu_e \frac{\partial E_{Fn}(x)}{\partial x}.$$

The open-circuit voltage theorem is based upon the values of the electron and hole quasi-Fermi levels E^0_{Fn} and E^0_{Fp} that would occur in the intrinsic layer material in isolation (i.e. without gradients or electric fields that would transport electrons and holes in space). Assuming ideal electrodes (the p and n layers), the open-circuit voltage eV_{OC} is

$$eV_{OC} = E^0_{Fn} - E^0_{Fp}. \tag{9}$$

I am not aware of any formal treatment of this theorem, but the basic idea has been in use for many years [10–12]. This idea is that photocarrier generation in a material may be viewed as creating two electronic reservoirs with differing chemical potentials. Electrons in the conduction band are one such reservoir; holes in the valence band are the second. Under open-circuit conditions, the n-layer serves as an ideal electrode permitting us to measure E_{Fn}; similarly, the p-layer simply serves as an ideal electrode permitting us to measure E_{Fp}. A voltmeter connected to the n- and p-layers then measures $(E_{Fn} - E_{Fp})/e$.

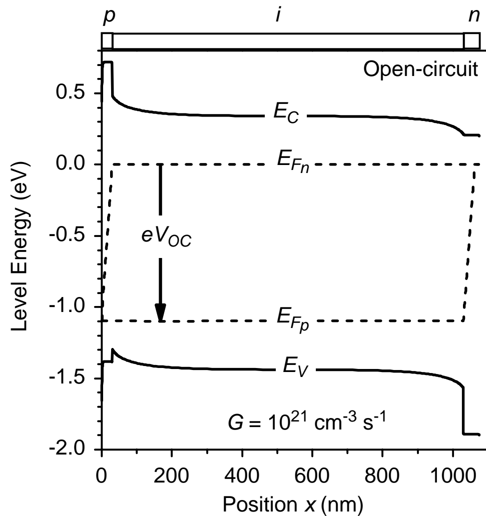

Fig. 5. Electronic level profiles calculated for a *pin* diode under illumination (open-circuit). The conduction and valence bandedges E_C and E_V and the electron and hole quasi-Fermi levels E_{Fn} and E_{Fp} are illustrated. Note the relation of the measured open-circuit voltage to the quasi-Fermi level splitting, and the convergence of the quasi-Fermi levels in the electrode layers. The hole mobility was $\mu_h = 10^{-4}\,cm^2/V\,s$; otherwise the parameters are the same as for Fig. 3.

In Fig. 5 we show the profiles for the valence and conduction bandedges E_V and E_C and for the quasi-Fermi levels E_{Fp} and E_{Fn} based on a full computer simulation. There is a broad region across the middle of the cell where the quasi-Fermi levels are constant, so the theorem may be applied. The separation of the two quasi-Fermi levels in this region is 1.09 eV; the open-circuit voltage calculated by the simulation is 1.0977, which is certainly quite close to the results anticipated from the theorem. The conduction and valence bandedges are not quite constant, even in the middle of the cell. Simulations with thicker cells do show more constancy in the bandedge positions, and the quasi-Fermi levels remain essentially the same.

The regions near the p/i and n/i interfaces are also interesting. Notice that the quasi-Fermi levels, which are well separated in the intrinsic layer, converge to the true Fermi energy in the electrode layers. Our implementation of "ideal" electrodes uses larger bandgap materials than for the intrinsic layer, and assumes that there is no photogeneration in these layers. For the *p*-layer, most of the bandgap difference occurs at the conduction band. This conduction band offset suppresses "thermionic emission" of electrons from the intrinsic layer into the *p*-layer [13,14]; thermionic emission at this interface leads to a substantial decrease in the measured V_{OC} compared to the ideal, intrinsic-layer dominated value. The *n*-layer choice is symmetrical, although in this case the choice has essentially no effect on V_{OC}. The relative insensitivity of V_{OC} to the *n*-layer parameters is a consequence of the fairly large electron mobility assumed by the simulation.

2.5. Analytical estimate: V_{OC}

Given this theorem, we now calculate V_{OC} for the present model of a *pin* cell. In electrically neutral material, $n = p$. Under illumination, the densities may be calculated by equating the rate of generation G with the rate of recombination $R = npb_R$:

$$\begin{aligned} R &= npb_R = G, \\ n &= p = (G/b_R)^{1/2}, \\ E^0_{Fn} &= E_C + \frac{kT}{2}\ln\left(\frac{G}{b_R N_C^2}\right), \\ E^0_{Fp} &= E_V - \frac{kT}{2}\ln\left(\frac{G}{b_R N_V^2}\right). \end{aligned}$$

We are neglecting thermal processes, which generate carriers in the dark. From the V_{OC} theorem we obtain:

$$eV^0_{OC} = E_G + kT\ln\left(\frac{G}{b_R N_C N_V}\right). \tag{10}$$

It is important to note that V^0_{OC} is independent of the electron and hole mobilities, and that this formula accounts naturally for the fact that V_{OC} depends little on thickness. The solid line approximating V_{OC} in Fig. 4 was calculated using this expression; it accounts very well for the results from the full computer simulation (shown as circular symbols).[2]

2.6. Analytical estimate of the saturated power density

Fig. 4 shows that the power delivered by a cell reaches a saturation value for cells with sufficiently thick intrinsic layers. In this section we present an analytical estimate for this saturated power density. Although we do not illustrate it here, for extremely thick cells the power will ultimately decline; this issue is treated briefly in Appendix B.

We first examine the profile of the electric field shown in Fig. 6 as it was calculated using the full computer simulation. The dashed curve indicates the field-profile under open-circuit conditions. Very near the p/i interface, there is a region with a quite large electric field. At first glance this field suggests that there must be some violation of the fact that there is no current in the cell under open-circuit conditions. Hole photocarriers in this high field region drift rapidly towards the p-layer. However, this drift simply cancels the diffusion of holes out of the p-layer, and the net current (drift-diffusion) remains zero. The field across the “back” of the cell is nearly zero.

[2] Indeed, the approximation works too well. In deriving the formula for V_{OC}, we assumed that there is a region with zero electric-field in the middle of the cell. Although we do not explore this in detail, this assumption breaks down for the thinnest cells in Fig. 4, but the value for V_{OC} still applies. It is likely that a derivation for V_{OC} even more general than the one described here must exist.

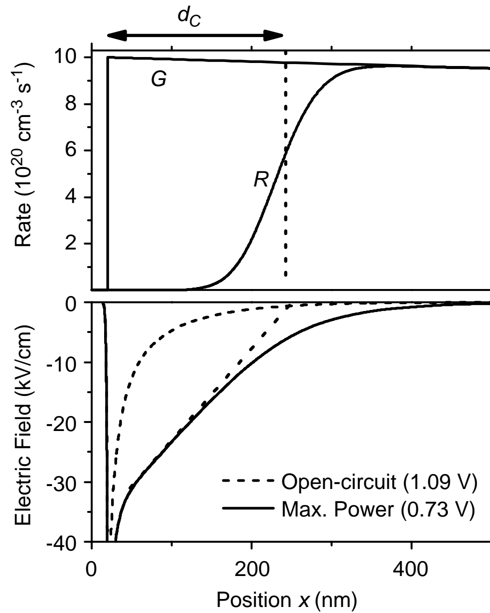

Fig. 6. Calculated profiles of the electric field and collection rate for an illuminated *pin* solar cell biased at its "maximum power point". The *p*-layer lies between 0 and 20 nm; the intrinsic layer is 5000 nm thick, of which about 500 nm are shown. $T = 300$ K. The hole mobility was $\mu_h = 10^{-4}$ cm^2/V s; otherwise the parameters are the same as for Fig. 3.

When the cell is biased at its maximum power point, the electric field penetrates more deeply into the cell, and net current is flowing. As can be seen, there is a reasonably linear decline of the field towards zero at a depth that we identify as the collection width d_C. It is worth noting that the area of this graph lying between the open-circuit and maximum-power curves corresponds to the difference $V_{OC} - V_{MP} = 0.36$ V.

A first estimate of the current that flows in the external bias circuit may be obtained by calculating the rate at which holes are generated within this collection zone: $j \approx eGd_C$. The presumption is that every such hole reaches the *p*-layer and is collected there, and that holes generated in the low-field region will recombine with electrons instead of being collected. Because the electrons are assumed to be far more mobile than the holes, the necessary electron current that must flow across the low-field zone can be driven by a negligible electric potential drop.

The presumption that holes generated within the collection zone are collected as photocurrent is consistent with the upper panel in Fig. 6. This panel illustrates the generation rate profile $G(x)$ in the calculation (essentially a constant) and the recombination profile $R(x)$. Deep in the device, for $x > d_C$, all photocarriers that are generated recombine without being collected (i.e. $G = R$). Near the p/i interface, for $x < d_C$, photocarriers are mostly collected. There is a transition region that we attribute to carrier diffusion processes; we discuss these shortly.

d_C may be estimated analytically using an elementary version of the "regional approximation" of Crandall [15]. As suggested by Fig. 6, the electric field declines essentially linearly to zero with depth, which corresponds to a uniform charge density ρ within collection zone (and zero beyond it). A uniform charge density is the correct solution to the set of semiconductor modeling equations in the collection region:

$$\frac{\partial J_h}{\partial x} = e(G - R) \qquad \text{(continuity equation)},$$

$$J_h(x) = \rho(x)\mu_h F(x) \qquad \text{(drift relation)},$$

$$\frac{\partial F(x)}{\partial x} = \frac{\rho(x)}{\varepsilon\varepsilon_0} \qquad \text{(Poisson's equation)}.$$

To evaluate the uniform charge density solution ρ $(0<x<d_C)$, consider the field and current density at $x=0$. From Poisson's equation we obtain:

$$F(0) = -\rho d_C/\varepsilon\varepsilon_0.$$

From the continuity equation (with $R=0$):

$$J_h(0) = -eGd_C$$

and from the drift relation:

$$J_h(0) = \rho\mu_h F(0) = -\rho^2\mu_h d_C/\varepsilon\varepsilon_0.$$

We obtain

$$\rho = \{e\varepsilon\varepsilon_0 G/\mu_h\}^{1/2}. \tag{11}$$

The collection width d_C is determined by ρ (which is independent of voltage) and the electric potential ΔV across the collection width. From our original assumption of a linear dependence of field upon depth

$$F(x) = -\frac{\rho d_C}{\varepsilon\varepsilon_0}\left(1 - \frac{x}{d_C}\right) \quad (0<x<d_C),$$

we obtain (from the definition $F(x)=-\partial V/\partial x$) that

$$\Delta V = V(d_C) - V(0) = d_C^2\rho/2\varepsilon\varepsilon_0$$

and hence

$$d_C = (\Delta V)^{1/2}(4\mu_h\varepsilon\varepsilon_0/eG)^{1/4}. \tag{12}$$

We need to evaluate d_C for the potential corresponding to maximum power. The output power density is given by $P(V)=-J(V)V$. $J(V)$ may be identified with the hole current J_h at $x=0$, which is $-eGd_C$. ΔV is the difference between the open-circuit voltage V_{OC} and the applied potential V:

$$\Delta V = V_{OC} - V$$

Thus $P(V) \propto (V_{OC} - V)^{1/2} V$, which reaches its maximum at $V = \left(\frac{2}{3}\right) V_{OC}$. From $J = -eGd_C$ and $P = -JV$, we obtain:

$$P = ((2/3)V_{OC})^{3/2}(\mu_h \varepsilon\varepsilon_0 (eG)^3)^{1/4} \quad (1)$$

and

$$d_C = ((2/3)V_{OC})^{1/2}(\mu_h \varepsilon\varepsilon_0 / eG)^{1/4}. \quad (5)$$

In Fig. 7 we have illustrated this expression for the power density as a function of the hole mobility μ_h along with the results from full computer simulation. For hole mobilities less than $10^{-2}\,cm^2/V\,s$, the agreement between the approximation and the analytical calculation is excellent. As the hole mobility increases, there is an obvious deviation, and for $\mu_h = 1$ the computer simulation predicts a power density that is 30% larger than the analytical approximation.

Most of the difference between the analytical approximations and the computer simulation may be attributed to our neglect of photocarrier diffusion processes. In the lower panel of Fig. 7 we have graphed the width of the depletion zone, along with the *ambipolar diffusion length* L_{amb}. L_{amb} estimates how far photocarriers diffuse before recombining in a region that is free of external electric fields. The formula for L_{amb} is derived in many textbooks; an adequate approximation using the present

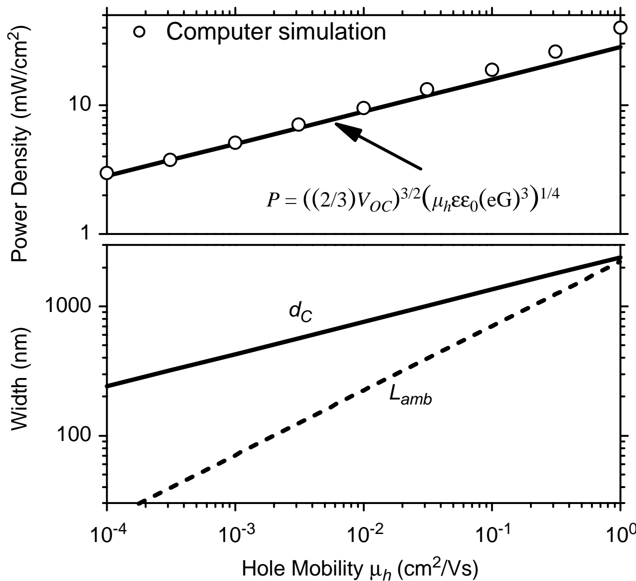

Fig. 7. (*upper*) Power density (for thick solar cells) delivered at the maximum power point as a function of the hole mobility. The solid line is based on an analytical estimate of the collection width d_C. (*lower*) Collection width d_C and ambipolar diffusion length L_{amb} as a function of hole mobility. Power estimates neglecting diffusion are reasonably accurate as long as L_{amb} is much smaller than d_C.

notation is

$$L_{\mathrm{amb}} \approx \left\{ 4(kT/e)^2 \frac{\mu_{\mathrm{h}}^2}{Gb_{\mathrm{R}}} \right\}^{1/4}. \tag{13}$$

We derive this formula in Appendix C. Note that L_{amb} increases more rapidly with the hole mobility than does d_{C}, and that $d_{\mathrm{C}} \approx L_{\mathrm{amb}}$ for $\mu_{\mathrm{h}} = 1\,\mathrm{cm^2/V\,s}$. These aspects are qualitatively consistent with the deviation between the computer simulations and the drift-zone approximation. We have examined the simple modification of adding the ambipolar diffusion length to d_{C} to estimate the total current. For $\mu_{\mathrm{h}} = 1\,\mathrm{cm^2/V\,s}$, this approximation yielded a power density about 50% larger than that calculated using the computer simulation. We have not developed a more satisfactory approximation incorporating diffusion.

2.7. Analytical estimate: power density for thin cells

Crudely speaking, for thin cells the power density is $eGdV_{\mathrm{OC}}$. This expression corresponds to saying that the fill-factor FF = 1, which is an unattainable ideal. An improved estimate can be made as follows [10]. We assume that, as the voltage across the cell is reduced from V_{OC}, and as photocarrier collection commences, the recombination rate R of electrons and holes simply falls below the generation rate G throughout most of the cell. Then the current density is

$$j(V) = eGd\left(1 - \frac{R(V)}{G}\right),$$

where d is the thickness of the intrinsic layer.

We can roughly estimate the applied potential associated with a given level of recombination by applying Eq. (4), but using the recombination rate R instead of the generation rate G to obtain an estimate at an arbitrary voltage V. This is a very strong approximation.

$$eV \approx E_G + kT\,\ln\left(\frac{R}{b_{\mathrm{R}}N_{\mathrm{C}}N_{\mathrm{V}}}\right),$$

$$e(V_{\mathrm{OC}} - V) = kT\,\ln\frac{G}{R},$$

$$J(V) = eGd(1 - \exp(-e\Delta V/kT)),$$

$$P = V \bullet J(V).$$

Maximizing the expression for the power, we obtain the result for the potential V_{m} at the maximum power-point:

$$(e/kT)V_{\mathrm{m}} = (e/kT)V_{\mathrm{OC}} - \ln(1 + (e/kT)V_{\mathrm{m}}).$$

For $b_{\mathrm{R}} = 10^{-9}\,\mathrm{cm^3/s}$, we previously estimated $V_{\mathrm{OC}} = 1.09\,\mathrm{V}$. Solving the expression above by iteration, we obtain $V_{\mathrm{m}} = 0.997\,\mathrm{V}$, which is fairly close to the value obtained by simulation $V_{\mathrm{m}} = 0.97\,\mathrm{V}$ for a 250 nm cell.

Since for sufficiently thin cells the short-circuit density $J_{SC} = eGd$, we can also estimate the FF for thin cells:

$$FF \approx (V_m/V_{OC})(1 - \exp(-e(V_{OC} - V_m)/kT)). \quad (14)$$

For the same numerical values, we obtain FF = 0.89. This is somewhat larger than the value from simulation FF = 0.83; we have not explored more complex approximations.

2.8. Discussion

A fairly common approach to studying photodiodes is to calculate the *J–V* relation in the dark, and then to assume that the *J–V* relation under illumination may be obtained by superposition: $J_{illuminated} = J_{dark}(V) - J_{photo}$ of the dark current and a voltage-independent photocurrent. This approach is incorrect for very low-mobilities; it assumes that the electric-field is unmodified by light, which is certainly not true for the present models. In addition, two earlier analyses have assumed a uniform electric field [16,17]. These analyses apply to cells in which the carrier mobility is large enough that it does not limit the power output; in this paper we have chosen to examine the low-mobility region.

Crandall [15] has done a comprehensive analysis of the regional approximation including space-charge effects. He found a space-charge limited regime that was independent of recombination; Section 2.6 of the present paper is essentially a more elementary version of his analysis. Crandall's more general equations include an analytical treatment of the transition to a recombination-limited cell.

We noted earlier that the power density saturates for significantly smaller thicknesses than does the short-circuit current density J_{SC} or the fill-factor. The reason for this difference is that the electric potential across the cell is larger under short-circuit conditions than it is at the maximum power point. Photocarriers that are deeper in the cell than d_C may thus be collected under short-circuit conditions, but this additional collection does not contribute to power generation.

3. The pin structure with bandtail traps

In the previous section we analyzed a model with specified electron and hole mobilities, and we found that a fairly good understanding of the resulting solar cell could be achieved by considering the space-charge that builds up due to slowly drifting low-mobility, photocarriers. However, we proposed no mechanism to explain either the small magnitudes of the mobilities or the asymmetry of the electron and hole mobilities.

Non-crystalline semiconductors do tend to have fairly low band mobilities. The best documented case is that of hydrogenated amorphous silicon, for which the electron band mobility is about $2\,cm^2/Vs$ [18,19]. The reduction of this mobility compared to the value in crystal silicon (around $1800\,cm^2/V\,s$ at 300 K) is undoubtedly an effect of the absence of long-range order, although there is no

conclusive theoretical calculation of the magnitude of this mobility in amorphous silicon.

In actual practice, the effective (or "drift") mobility is further reduced, often quite dramatically, by *trapping* of carriers into localized states between the bandedges. More particularly, several amorphous semiconductors have quite low drift mobilities because of localized "bandtail" levels that lie just above the valence bandedge or just below the conduction bandedge. These localized states capture and immobilize holes and electrons, respectively. The carriers remain in the traps until they are thermally excited back into the bands (or, alternatively, until they recombine). The trapping events reduce the effective mobility of the carriers, since the carriers spend relatively little time in band states (where they are mobile), and most of their time in traps (where they are immobile).

In 1981, research groups at the Massachusetts Institute of Technology [20] and at the Exxon Corporation Research Laboratories [21] discovered independently that a quite satisfactory account for drift-mobility measurements in amorphous As_2Se_3 and in a-Si:H could be given using an exponential distribution of these trap states. For the valence bandtail this means that the trap distribution vs. level energy is written:

$$g_V(E) = g_V^0 \exp\left(-\frac{E - E_V}{\Delta E_V}\right) \quad E > E_V. \tag{15}$$

The prefactor g_V^0 has the dimensions cm^3/eV. ΔE_V is the width of the valence bandtail, which was found to be around 50 meV in both materials. For a-Si:H, the conduction bandtail width is smaller (around 22 meV [22]), and indeed it is small enough that near room-temperature ($kT = 25$ meV) conduction bandtail trapping can be neglected.

In this section we present a model for a *pin* solar cell based on an absorber material with an exponential valence bandtail. To keep the model reasonably simple, we neglect electron trapping. As just noted, this is actually an acceptable approximation for a-Si:H near room-temperature (but a very poor one for a-As_2Se_3). As we shall see, the trapping of holes leads to quantitative changes in the behavior of cells compared to the low-mobility, but trap-free, case of the previous sections. The qualitative behavior of cells is nearly unchanged.

In addition to the parameters already introduced for the trap-free case, only one additional parameter (beyond the density of trapping states) is required for numerical simulation. This parameter is the "trapping coefficient" b_T, which describes the rate of capture of mobile holes (density p) by bandtail traps (density g): $R_{trap}=b_T pg$. A discussion of the parameters used in the present paper is given in Appendix D; they have been chosen to describe amorphous silicon.

3.1. Current–voltage relations for varying cell thickness

In Fig. 8 we show calculated solar cell parameters as a function of the absorber layer thickness. The valence bandtail width was 50 meV; other parameters are summarized in Appendix D. The qualitative similarity with Fig. 4, which shows calculations for the simpler, trap-free model, is unmistakable. In both cases V_{OC} is

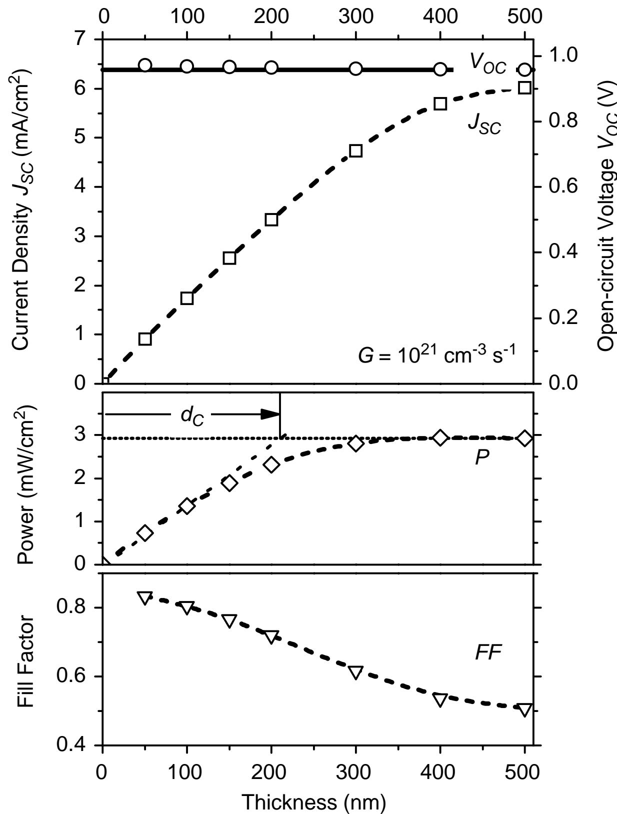

Fig. 8. Calculated solar cell parameters at 300 K for a model with exponential valence bandtail traps (50 meV width). The short-circuit current density J_{SC}, open-circuit voltage V_{OC}, power density P (at the maximum power point), and the fill factor are shown for varying absorber layer thickness. The solid line is an analytical approximation to V_{OC}. d_C is the collection width under maximum power conditions; the dashed lines are just guides. Modeling parameters include $\mu_h^0 = 1\,cm^2/V\,s$, $N_V = N_C = 5 \times 10^{20}/cm^3$, $b_R = 10^{-9}\,cm^3/s$, $b_T = 2 \times 10^{-10}\,cm^3/s$ (see Appendix D).

nearly independent of thickness, but the power saturates for thicknesses beyond the collection width d_C. The saturation thresholds are different, and correspond to different saturated powers (about $8\,mW/cm^2$ for Fig. 4, and about $3\,mW/cm^2$ for Fig. 8).

Fig. 4 was obtained using $\mu_h = 10^{-2}\,cm^2/V\,s$. Fig. 7, which showed how the saturated power increased with μ_h, indicates that a power of $3\,mW/cm^2$ would have resulted if the hole mobility were $2 \times 10^{-4}\,cm^2/V\,s$. It is interesting to compare this mobility with some kind of mobility corresponding to the situation with bandtail traps. For exponential bandtail trapping, it is incorrect to describe hole transport in terms of any specific mobility, but an average "drift-mobility" can be defined for a specific hole displacement L and electric field F [22]. The drift-mobility

corresponding to a particular ratio L/F is

$$\mu_h(L/F) = \mu_h^0 \left(\frac{L/F}{\mu_h^0/\nu} \right)^{1-1/\alpha},$$
$$\alpha \equiv \frac{kT}{\Delta E_V}. \tag{16}$$

The parameter ν is an "attempt-to-escape" frequency that describes the rate S at which a trapped carrier is thermally released; more specifically $S = \nu \exp(-\delta E/kT)$, where δE is the binding energy of the carrier to the trap. The ratio α is called the "dispersion parameter".

For the case of Fig. 8, holes drift about $L = 200$ nm (the collection width d_C) under conditions of maximum power output. Under the same conditions, the voltage dropped across the collection width is around $V_{OC}/3$, and the average electric field F is about $V_{OC}/3L = 1.6 \times 10^4$ V/cm. The corresponding ratio is $L/F = 1.25 \times 10^{-9}$ cm^2/V. The hole drift-mobility is about 8×10^{-3} cm^2/V s for this value of L/F; the necessary formulae are given in Appendix E. The magnitude is not too different than the value $\mu_h = 2 \times 10^{-4}$ cm^2/V s for the trap-free calculation, but it is clear that the simpler calculation is not an adequate quantitative guide to the calculation with bandtail traps.

3.2. Analytical estimate: open-circuit voltage

The derivation of an analytical estimate for V_{OC} along the lines we previously used for the trap-free situation may be found in Appendix E. It is a bit messy, but here is the algebraic expression for eV_{OC}:

$$eV_{OC} = E_G + \frac{kT}{2} \left\{ \ln\left(\frac{G}{b_R N_C^2} \right) + 2 \ln\left(\frac{G}{b_T N_V^2} \right) - \frac{kT}{\Delta E_V} \ln \left[\frac{b_R}{b_T} \left(\frac{G}{b_T N_v^2} \right) \right] \right\} \tag{17}$$

In Fig. 8 we have illustrated the calculated value $V_{OC} = 0.97$ V based on this approximation, along with the results from the simulation. The agreement is very good.

It is worth remarking that these open-circuit voltages are reduced about 10% from the trap-free value (about 1.10 eV), and that eV_{OC} is substantially smaller than $E_G = 1.78$ eV for both the trap-free and the bandtail cases.

3.3. Effects of bandtail width

For the trap-free models, we studied how the saturated power output of a cell depended upon the hole-mobility. For the present, bandtail trapping model, the analogous dependence is that of the saturated power output upon the valence bandtail width ΔE_V. As the valence bandtail is narrowed, the hole drift-mobility increases, and we expect increased power.

In Fig. 9 we have illustrated how the saturated power output and the collection width d_C depend upon the valence bandtail width. d_C was determined using the procedure illustrated in Fig. 8. As one would expect from analogy with the trap-free

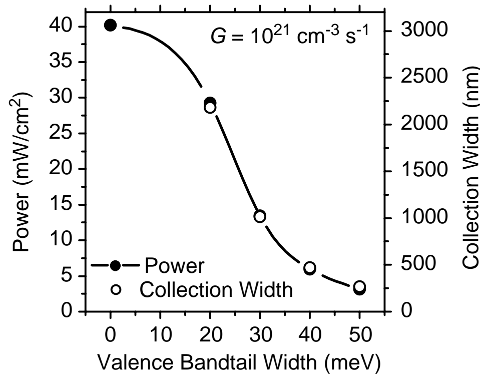

Fig. 9. Dependence of the saturated power output and of the collection width d_C for a *pin* solar cell upon the width of the exponential valence bandtail. Results were obtained by direct computer simulation for uniform photogeneration ($G = 10^{21}/\text{cm}^3/\text{s}$); excepting the valence bandtail width, the modeling parameters are the same as for Fig. 8.

case, increasing the drift-mobility increases the power output. The physical mechanism is exactly the same as for the trap-free case: the space-charge of drifting holes sets a upper limit to the size of the region from which holes can be collected. The faster the drift of holes, the less the space-charge at a given level of photogeneration, and the larger the collection region.

It may be useful to note that the case $\Delta E_V = 0$ corresponds precisely to the trap-free case (with $\mu_h = 1\,\text{cm}^2/\text{Vs}$). The increase in power (under uniform generation) as ΔE_V is reduced from 20 to 0 meV is about 30%; this is relatively modest compared to the nearly tenfold increase as ΔE_V fell from 50 to 20 meV. The reason that the increase in power is arrested is that, when the thermal energy kT is larger than ΔE_V, bandtail trapping effects are actually fairly small.

4. Implications for solar conversion by amorphous silicon

In the previous section, the discussion of solar cells incorporating intrinsic, absorber layers with exponential valence bandtail traps was intentionally general, and we described only the simplest case of uniform photogeneration. However, the parameters were chosen so that the results can easily be adapted to hydrogenated amorphous silicon, for which $\Delta E_V \approx 48\,\text{meV}$ [21,23]. The principal difficulty in applying the results from the last section is that the photogeneration in a solar cell is certainly not uniform, as was assumed; in this section we adapt the model to the case of solar illumination.[3]

[3] Multijunction structures consisting of two or three cells stacked vertically are used for high-efficiency amorphous silicon-based cells. The full solar spectrum reaches only the top cell, so the present calculation can only be applied directly to this cell. We have also assumed that the back surface of the cell is non-reflecting. A high-efficiency design for a single *pin* junction solar cell would incorporate both a back-reflector and other optical enhancements such as substrate texturing.

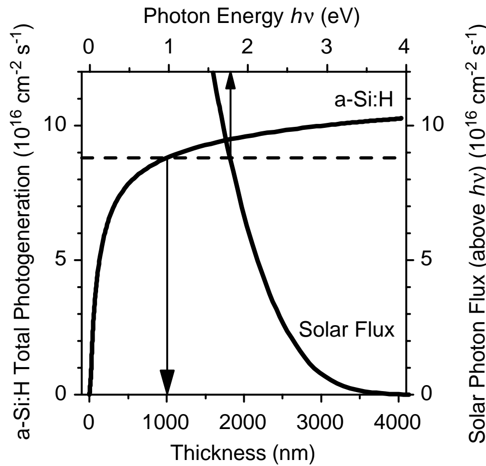

Fig. 10. The curve labeled "solar flux" indicates the flux of photons in sunlight with photon energies above $h\nu$; the corresponding axes are at the top and right of the figure. The curve labeled "a-Si:H" indicates the total photogeneration density (cm^{-2}/s) for varying thicknesses of a-Si:H under solar illumination. The figure illustrates that a total photogeneration of $8.8 \times 10^{16}\,cm^{-2}/s$ in a 1000 nm film corresponds to the solar photon flux above 1.8 eV.

In Fig. 10 we have illustrated the total photon flux in the solar spectrum above a specified photon energy $h\nu$.[4] We have also illustrated the total photogeneration that occurs via absorption of this flux in a-Si:H as a function of thickness. We are neglecting reflection either at the front or the back of the a-Si:H layer. Additionally, the absorption properties of a-Si:H do vary somewhat with its preparation conditions; the values we have chosen are fairly typical [24]. Note that, for a film that is 1000 nm thick, the total photogeneration is about $8.8 \times 10^{16}\,cm^{-2}/s$. As illustrated in the figure, this value corresponds to the solar flux with photon energies greater than 1.8 eV, and indeed nearly all of the photons absorbed by the film do have energies larger than this value. The figure also illustrates the important fact that increasing the thickness of a-Si:H beyond a few hundred nm yields fairly little additional absorption of the solar spectrum.

Fig. 11 illustrates the main solar cell parameters as a function of thickness; results are shown for a 50 meV valence bandtail width and for no valence bandtail (0 meV). For reference, there is about $100\,mW/cm^2$ of solar irradiance available for full solar illumination. The cell is illuminated through the *p*-layer; because holes are the lower mobility photocarrier, it is advantageous that they should be generated closer to the *p*-layer, which is their destination. The power would be substantially reduced for

[4] Hemispherical irradiance was based on the American Society for Testing and Materials (ASTM) Table G159-98, "Standard Tables for Reference Solar Spectral Irradiance at Air Mass 1.5: Direct Normal and Hemispherical for a 37° Tilted Surface."

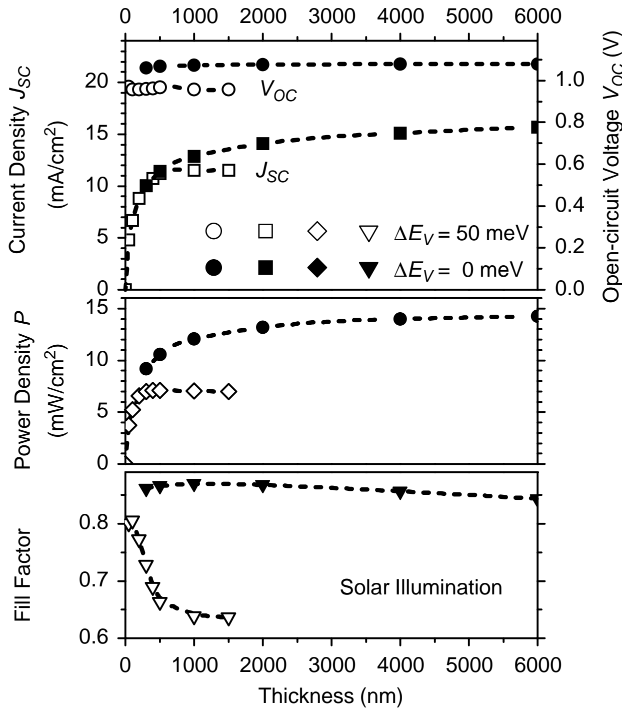

Fig. 11. Calculated *pin* solar cell parameters for a model with exponential valence bandtail traps (300 K). The calculation is for solar illumination through the *p*-layer; the cell has no back reflector. The short-circuit current density J_{SC}, open-circuit voltage V_{OC}, power density (at the maximum power point) P, and fill factor are shown for varying intrinsic layer thickness. Results are illustrated for two different valence bandtail widths ΔE_V; otherwise the modeling parameters are the same as for Fig. 8.

illumination through the *n*-layer [1–3]. Reflection of light at the front and back interfaces of the cell is neglected.

The results with a 50 meV bandtail in this figure may be directly compared with Fig. 8, which was calculated for uniform photogeneration. The short-circuit currents and powers are roughly twice as large as for the earlier figure, which merely reflects the somewhat arbitrary choice of $G = 10^{21}$ cm^{-3}/s for the uniform photogeneration in Fig. 8. The open-circuit voltages are similar; this is sensible, since V_{OC} varies only logarithmically with intensity. There is about a 13% increase in V_{OC} without the bandtail (0 meV width). The improvement may be satisfactorily explained using Eq. (17). With the 50 meV bandtail, the output power saturates for thicknesses greater than about 200 nm, as would be anticipated given the collection width (about 250 nm) illustrated in Fig. 9. Without the bandtail, the power is larger, with the improvement being larger for thicker cells. These effects originate in the increase in collection width as the bandtail narrows. The highly inhomogeneous photogeneration evident in Fig. 10 leads to a much slower increase in the power with thickness than was illustrated for uniform photogeneration (Fig. 8).

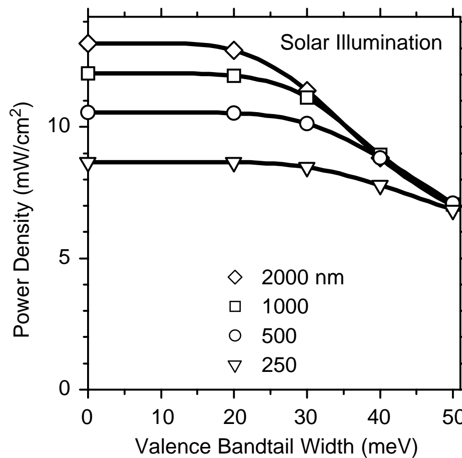

Fig. 12. Calculated power density of a-Si:H based *pin* solar cells under solar illumination as a function of valence bandtail width; results are indicated for four intrinsic layer thicknesses. The cell has no back reflector. Except for the bandtail width, the modeling parameters are the same as for Fig. 8.

In Fig. 12 we plot the power output as a function of the valence bandtail width; curves are shown for four thicknesses ranging from 250 to 2000 nm. The four curves converge for a 50 meV bandtail, which simply reflects that the collection width is less than 250 nm for this bandtail. As the bandtail declines, the collection width increases, so that thinner cells generate less power than thicker cells; the increase in power with thickness is much lower than for cells with uniform photogeneration.

Experimentally, the bandtail width that applies to "typical" a-Si:H is in the range 45–50 meV. In Fig. 13 we have illustrated experimental results for a series of a-Si:H solar cells with varying thickness, as well as the predictions of the present model for bandtail widths of 40 and 50 meV [1]. There have been several reports [25–27] of improvement in the hole drift-mobilities of a-Si:H. We envision that an improvement corresponding to $\Delta E_V = 40$ meV may well be possible. As illustrated, this improvement would correspond to a power output of about 9 mW/cm^2, but would require a 500 nm cell to exploit.

We conclude by commenting briefly on the decline in the power output of a-Si:H-based solar cells as they become "light-soaked". We believe that the calculations in this paper adequately describe the initial behavior of a-Si:H cells (before they have become light-soaked). In simple structures such as we have described in this paper, the decline in power is about 30% for thicker cells and very long solar exposures [1–3]. It is believed that this effect is due to the creation of dangling bond defects by photocarrier recombination in a-Si:H. The defects subsequently trap photocarriers, presumably leading to a decline in the effective collection width for the cell; light soaking has relatively little effect on V_{OC}. The present calculations do not address this effect. They indicate the ultimate conversion efficiencies for cells for which

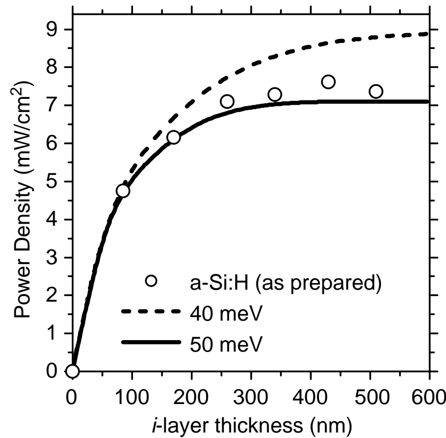

Fig. 13. The output power densities under solar illumination for a-Si:H solar cells of varying thickness prepared at United Solar Systems Corp. [1] are indicated by the symbols. The cells were in their ''as-prepared'' state, and had not yet been significantly exposed to sunlight. Model calculations based on exponential valence bandtails of 40 and 50 meV width are indicated by the dashed and solid lines; the remaining modeling parameters are the same as for Fig. 8.

dangling bond trapping is unimportant, and they show how narrowing of the valence bandtail improves this limit. We do not presently know whether such narrowing will improve cells that are in the light-soaked state, which must await further research.

Acknowledgements

Stanford Ovshinsky's leadership in the science and industry dedicated to clean and inexpensive solar energy has been an inspiration to the author. This research was supported by the Thin Film Photovoltaic Partnership of the National Renewable Energy Laboratory (NDJ-2-30630-24).

Appendix A. AMPS implementation (trap-free model)

The recombination parameter in ©AMPS PC is a ''cross-section'' σ_R which is related to the recombination coefficient b_R by $\sigma_R = v_{th} b_R$, where $v_{th} = 10^7$ cm/s is a conventional ''thermal velocity''. The use of cross-sections is conventional in semiconductor physics, although unlikely to have much meaning for low-mobility materials.

©AMPS PC does not permit an exact translation of the trap-free model in the first section. There is no parameter in AMPS describing the direct recombination process of free electrons and free holes. The particular implementation for the present

simulations assumes narrow exponential bandtails (width = 0.01 eV), and a density-of-states prefactor GD0 = GA0 = N_C/0.025. GD0 and GA0 are AMPS parameter names for the density prefactors describing the exponential bandtails. 0.025 eV is a nominal value for kT at room-temperature. The ratio N/n of the density of carriers N that are trapped in this narrow bandtail to the density of free electrons n is obtained as follows. One calculates the energy-integral of the exponential trap distribution (rising towards the bandedge) times the Boltzmann factor (declining as the bandedge is approached). This density is divided by the effective density N_C of the band. For a 0.01 eV bandtail width we obtain the ratio of trapped electrons to free electrons to be $\frac{2}{3}$.

To adjust the AMPS parameters to give the same results as the analytical calculation, I used the following substitutions. To get the total space-charge to be correct for a given quasi-Fermi level position, I set N_C and N_V to $\frac{3}{4}$ of the value used for the analytical approximation; GA0 and GD0 were reduced by the same factor. To get the same recombination rate, b_R needs to be increased. For a given space-charge of electrons, only $\frac{3}{5}$ can recombine, and only $\frac{2}{5}$ of the holes are targets. On the other hand, AMPS treats electron-to-trapped-hole and hole-to-trapped-electron recombination separately. Therefore b_R was increased by the factor $(\frac{5}{3})\,(\frac{5}{2})/2 = \frac{25}{12}$. Finally, since only $\frac{3}{5}$ of the space-charge is mobile, we need to increase the mobilities by a factor $\frac{5}{3}$ to get the correct currents.

Appendix B. Decline of power for extremely thick cells

We have shown several figures that suggest that, for thick cells, the power reaches a saturation value that is independent of thickness. Even for the uniform photogeneration model, this is not strictly true. For sufficiently large intrinsic layer thickness d, the power will decline due to Ohmic losses of moving the photocurrent through the ‘‘back’’ region of the cell. Denoting the photoconductivity of this region as σ_{photo}, the potential drop across the back due to a current density J is $V_{Ohmic} = Jd/\sigma_{photo}$. For this Ohmic potential drop to be negligible, we require that $d \ll \sigma_{photo}(V_{OC} - V)/J$.

For the ‘‘trap-free’’ case it is fairly straightforward to evaluate this thickness. For $G = 10^{21}/\text{cm}^3/\text{s}$, $b_R = 10^{-9}\,\text{cm}^3/\text{s}$, and $\mu_e = 20\,\text{cm}^2/\text{V s}$, we obtain $\sigma_{photo} = 3.2 \times 10^{-3}/\Omega/\text{cm}$. For the case of Fig. 4, thick cells have $V_{OC} - V = 0.3$ V and $J = 1.2 \times 10^{-2}\,\text{A/cm}^2$ at the maximum power point. The limiting thickness is 8×10^{-2} cm; the largest thickness included in the figure was 2×10^{-4} cm.

Appendix C. Ambipolar diffusion length

L_{amb} is the length scale characterizing how far a hole will diffuse before recombining with an electron; this length is the square-root of the product of the *ambipolar diffusion constant* D_{amb} [8] and the rate ν_R at which a hole

recombines:

$$L_{\rm amb} = \{D_{\rm amb}/v_{\rm R}\}^{1/2},$$
$$D_{\rm amb} = \frac{n+p}{(n/D_{\rm h})+(p/D_{\rm e})},$$
$$L_{\rm amb} \approx \left\{2(kT/e)\frac{\mu_{\rm h}}{nb_{\rm R}}\right\}^{1/2} = \left\{4(kT/e)^2\frac{\mu_{\rm h}^2}{Gb_{\rm R}}\right\}^{1/4}.$$

We have used the Einstein relation $D=(kT/e)\mu$ that connects carrier diffusion coefficients and mobilities, and we have assumed that $D_{\rm h} \ll D_{\rm e}$.

Appendix D. Solar cell modeling parameters (with valence bandtail trapping)

We have chosen parameters based on a-Si:H. We are neglecting alloyed materials such as a-SiGe:H that are based on a-Si:H. Even without alloying effects, there is variability in the properties of a-Si:H, so the present choices should be considered as "typical" instead of as definitive.

E_G: The "electrical" bandgap E_G in a given amorphous silicon based material is not precisely established. Our value (1.78 eV) is somewhat smaller than estimates from internal photoemission [28], but is closer to estimates from temperature-dependent $V_{\rm OC}$ measurements [29].

$\Delta E_{\rm V}$, $\mu_{\rm h}^0$, $N_{\rm V}b_{\rm T}$: These three parameters may be obtained from hole time-of-flight measurements such as the 1994 paper of Gu et al. [23]. This paper proposed $\Delta E_{\rm V} = 48$ meV, $\mu_{\rm h}^0 = 0.27\,{\rm cm}^2/{\rm V\,s}$, and an attempt-to-escape frequency $v = 7.7\times10^{10}$ s; the product $N_{\rm V}b_{\rm T}$ is equal to v. Unpublished work from Syracuse University [27] indicates that hole drift mobilities have increased in more modern samples, although no detailed description yet exists for how and why the three time-of-flight parameters vary in differing forms of a-Si:H. For simplicity, we use a valence band mobility $\mu_{\rm h}^0 = 1\,{\rm cm}^2/{\rm V\,s}$ and $v = 10^{11}$/s; the bandtail width is treated as a variable in the present work.

$N_{\rm V}$, $g_{\rm V}^0$, $b_{\rm T}$: Little is known about the value for $N_{\rm V}$; we used $5\times10^{20}/{\rm cm}^3$ based on the temperature-dependence of $V_{\rm OC}$ [29]. This choice, in conjunction with the value for v, implies $b_{\rm T} = 2\times10^{-10}\,{\rm cm}^3/{\rm s}$. Time-of-flight also constrains the ratio $g_{\rm V}^0/N_{\rm V}$; we used $g_{\rm V}^0 = 10^{22}/{\rm cm}^3/{\rm eV}$. This issue is discussed further just below.

$b_{\rm R}$: The recombination coefficient $b_{\rm R}$ is about $10^{-9}\,{\rm cm}^3/{\rm s}$ based on high-intensity recombination measurements [30,31].

$N_{\rm C}$, $\mu_{\rm e}$: $N_{\rm C}$ is not directly known; we arbitrarily used $N_{\rm C} = N_{\rm V}$. From electron time-of-flight measurements, $\mu_{\rm e}$ is $2\,{\rm cm}^2/{\rm V\,s}$ [18,19]. Neither parameter strongly affects results.

D.1. Relation of N_V and $g(E)$

We derive the relationship of the band density-of-states parameter $N_{\rm V}$ when the bandedge lies within an exponential density of states. Assuming

that the bandedge is at $E=0$, the exponential density of states may be written:

$$g(E) = g_V^0 \exp(-E/\Delta E_V).$$

The effective density of states is

$$N_V = \int_{-\infty}^{0} g(E)\exp(E/kT)\,dE.$$

We obtain:

$$N_V = kTg_V^0\left(1 - kT/\Delta E_V\right)^{-1}. \quad (18)$$

This relationship is valid only for $kT < \Delta E_V$. When $kT > \Delta E_V$, the effective band density corresponds to states lying below the exponential region.

Appendix E. Drift mobilities and bandtail trapping

The time-dependent displacement of a hole is written as

$$L(t) = (\mu_h^0 E/v)\{vt\}^a,$$
$$\alpha \equiv \frac{kT}{\Delta E_V}.$$

The parameter v is an "attempt-to-escape" frequency that describes the rate R at which a trapped carrier is thermally released; more specifically $R = v\exp(0 - \delta E/kT)$, where δE is the binding energy of the carrier to the trap. The ratio α is called the "dispersion parameter". The drift-mobility corresponding to a particular ratio L/E is

$$\mu_h(L/E) = \mu_h^0\left(\frac{L/E}{\mu_h^0/v}\right)^{1-1/\alpha}.$$

Appendix F. Analytical derivation of V_{OC} (with valence bandtail trapping)

In this appendix we derive an analytical approximation for V_{OC} including valence bandtail trapping. We use the quasi-Fermi level approach that was described for the "no-traps" model. The present calculation is actually a simplification of one by Tiedje that incorporated both valence bandtail and conduction bandtail trapping [11].

F.1. Electron quasi-Fermi level

The derivation of the electron quasi-Fermi level E_{Fn} is nearly identical to that for the trap-free case. P is the density of holes in bandtail states; we are assuming that the density of mobile holes p in band states is much smaller than P.

$$nPb_R = G,$$
$$n = P,$$
$$n^2 = G/b_R,$$
$$n = (G/b_R)^{1/2},$$
$$n \equiv N_C \exp(-(E_C - E_{Fn})/kT),$$
$$E^0_{Fn} = E_C + kT \ln(n/N_C) = E_C + (kT/2)\ln\left(\frac{G}{b_R N_C^2}\right).$$

b_R now denotes the coefficient for electron capture by a trapped hole; the definitions of the remaining symbols are unchanged, as is the equation for the electron quasi-Fermi level.

F.2. Hole quasi-Fermi level

The first issue is the distribution of holes in the bandtail traps. This needs a figure to illustrate, but there are about N_V total traps in the bandtail that are distributed exponentially with a characteristic energy kT_V. Very deep in the bandtail, the occupancy by holes is kept to a rather low, constant value f by competition between capture of holes (coefficient b_T) and capture of electrons. A demarcation energy E_{Dp} may be defined as the level at which the occupancy of holes switches from the constant value f to an Boltzmann exponential as the valence band is approached.

$$f \equiv \frac{pb_T}{nb_R},$$
$$P \approx fN_V \exp(-(E_{Dp} - E_V)/kT_V).$$

The idea of the expression for P is that, if E_{Dp} were at the valence bandedge, then the density would be about fN_V. Since E_{Dp} is actually above the edge, the density is lower according to the exponential decay of the trap density.

Now, the demarcation energy may be calculated by equating the rate of emission of a trapped hole at E_{Dp} with the rate of electron capture by the same hole:

$$nb_R = \nu \exp(-(E_{Dp} - E_V)/kT),$$
$$P = n = fN_V \left(\frac{nb_R}{\nu}\right)^{kT/kT_V},$$

$$n = \frac{pb_T N_V}{nb_R}\left(\frac{nb_R}{v}\right)^{kT/kT_V} = p\left(\frac{nb_R}{v}\right)^{(kT/kT_V)-1},$$
$$\frac{pb_R}{v} = \left(\frac{nb_R}{v}\right)^{2-(kT/kT_V)}.$$

We have used the *detailed balance expression* $v = N_V b_T$. We can use the expression for p to get E_{Fp} in terms n and thus in terms of G.

$$p = N_V \exp(-(E_{Fp} - E_V)/kT),$$
$$E_{Fp} = E_V - kT \ln(p/N_V),$$
$$E_{Fp} = E_V - kT \,\mathrm{In}\left[\left(\frac{v}{N_V b_R}\right)\left(\frac{nb_R}{v}\right)^{2-(kT/kT_V)}\right],$$
$$E_{Fp} = E_V - kT \ln\left[\left(\frac{b_T}{b_R}\right)\left(\frac{(G/b_R)^{1/2} b_R}{v}\right)^{2-(kT/kT_V)}\right],$$
$$E_{Fp} = E_V - kT \,\mathrm{In}\left[\left(\frac{b_T}{b_R}\right)\left(\frac{Gb_R}{v^2}\right)^{1-(kT/2kT_V)}\right],$$
$$E_{Fp} = E_V - kT\, In\left[\frac{G}{b_T N_V^2}\right] + \frac{(kT)^2}{2kT_V}\,\mathrm{In}\left[\frac{b_R}{b_T}\left(\frac{G}{b_T N_V^2}\right)\right].$$

F.3. Open-circuit voltage

Here's the algebraic expression for eV_{OC}:

$$eV_{OC} = E_G + \frac{kT}{2}\left\{\ln\left(\frac{G}{b_R N_C^2}\right) + 2\ln\left(\frac{G}{b_T N_V^2}\right) - \frac{kT}{kT_V}\ln\left[\frac{b_R}{b_T}\left(\frac{G}{b_T N_V^2}\right)\right]\right\}. \quad (17)$$

Something interesting happens at $T = T_V$:

$$eV_{OC} = E_G + kT \ln\left(\frac{G}{b_R N_C N_V}\right).$$

This is the exact expression without trapping (from the first section); the factor b_T cancelled out. At $T = T_V$, the effects of hole trapping are essentially negligible, so this makes some sense. For $T > T_V$ the earlier derivation (without traps) is essentially correct even with the bandtail.

References

[1] S. Guha, in: R.A. Street (Ed.), Technology and Applications of Amorphous Silicon, Springer, Berlin, 1999, pp. 252–305.
[2] C.R. Wronski, D.E. Carlson, In: M. D. Archer, R. Hill (Eds.), Clean Electricity from Photovoltaics, World Scientific, Singapore, 2001.

[3] X. Deng, E.A. Schiff, in: A. Luque, S. Hegedus (Eds.), Handbook of Photovoltaics Engineering, Wiley, Chichester, in press.
[4] K. Petritsch, J.J. Dittmer, E.A. Marseglia, R.H. Friend, A. Lux, G.G. Rozenberg, S.C. Moratti, A.B. Holmes, Sol. Energy Mater Sol. Cells 61 (2000) 63.
[5] M. Grätzel, Pure Appl. Chem. 73 (2001) 459.
[6] N. Kopidakis, E.A. Schiff, N.G. Park, J. van de Lagemaat, A.J. Frank, J. Phys. Chem. B. 104 (2000) 3930.
[7] H. Zhu, S. Fonash, in: R.E.I. Schropp, et al. (Eds.), Amorphous and Microcrystalline Silicon Technology—1998, Materials Research Society, Symposium Proceedings, Vol. 507, Pittsburgh, 1998, p. 395.
[8] S.M. Sze, Physics of Semiconductor Device Physics, 2nd Edition, Wiley, New York, 1981.
[9] S. Fonash, Solar Cell Device Physics, Wiley, New York, 1981.
[10] W. Shockley, H.J. Queisser, J. Appl. Phys. 32 (1961) 510.
[11] T. Tiedje, Appl. Phys. Lett. 40 (1982) 627.
[12] A. Luque, A. Marti, Phys. Rev. Lett. 78 (1997) 5014.
[13] L. Jiang, S. Rane, E.A. Schiff, Q. Wang, Q. Yuan, in: H. M. Branz, et. al. (Ed.), Amorphous and Heterogeneous Silicon Films—2000, Materials Research Society, Symposium. Proceedings, Vol. 609, Pittsburgh, 2000, p. A18.3.
[14] E.A. Schiff, in Conference Record of the 29th Photovoltaic Specialists Conference, IEEE, New York, 2002, pp. 1086–1089.
[15] R.S. Crandall, J. Appl. Phys. 55 (1984) 4418.
[16] R.S. Crandall, J. Appl. Phys. 54 (1983) 7176.
[17] S. Hegedus, Prog. Photovolt. Res. Appl. 5 (1997) 151.
[18] E.A. Schiff, R.I. Devlen, H.T. Grahn, J. Tauc, S. Guha, Appl. Phys. Lett. 54 (1989) 1911.
[19] G. Juska, K. Arlauskas, J. Kocka, M. Hoheisel, P. Chabloz, Phys. Rev. Lett. 75 (1995) 2984.
[20] J. Orenstein, M.A. Kastner, V. Vaninov, Philos. Mag. B 46 (1982) 22.
[21] T. Tiedje, in: J. D. Joannopoulos, G. Lucovsky, (Eds.), Hydrogenated Amorphous Silicon II, Springer, New York, 1984.
[22] Q. Wang, H. Antoniadis, E.A. Schiff, S. Guha, Phys. Rev. B 47 (1993) 9435.
[23] Q. Gu, Q. Wang, E.A. Schiff, Y.M. Li, C.T. Malone, J. Appl. Phys. 76 (1994) 2310.
[24] L. Jiao, I. Chen, R.W. Collins, C.R. Wronski, N. Hata, Appl. Phys. Lett. 72 (1998) 1057.
[25] G. Ganguly, A. Matsuda, J. Non-Cryst. Solids 198–200 (1996) 1003.
[26] B.A. Korevaar, G.J. Adriaenssens, A.H.M. Smets, W.M.M. Kessels, H.Z. Song, M.C.M. van de Sanden, D.C. Schram, J. Non-Cryst. Solids 266–269 (2000) 380.
[27] S. Dinca, P. Rao, Q. Yuan, E.A. Schiff, C.R. Wronski, unpublished.
[28] I.S. Chen, C.R. Wronski, J. Non-Cryst. Solids 190 (1995) 58.
[29] K. Zhu, W. Wang, E.A. Schiff, unpublished.
[30] G. Juska, J. Kocka, M. Viliunas, K. Arlauskas, J. Non-Cryst. Solids 164–166 (1993) 579.
[31] P. Stradins, H. Fritzsche, P. Tzanetakis, N. Kopidakis, in: M. Hack, et al. (Eds.), Amorphous Silicon Technology—1996, Materials Research Society Symposium Proceedings, Vol. 420, Pittsburgh, 1996, p. 729.